

No Validation, No Problem: Predicting Model Performance from a Single Gradient

Fangzheng Wu
Tulane University
New Orleans, LA
fwu6@tulane.edu

Brian Summa
Tulane University
New Orleans, LA
bsumma@tulane.edu

Abstract

We propose a validation-free checkpointing signal from a single forward-backward pass: the Frobenius norm of the classifier-head gradient on one detached-feature batch, $\|g\|_F = \|\nabla_W \mathcal{L}\|_F$. Across ImageNet-1k CNNs and Transformers, this proxy is strongly negative with Top-1 and positive with loss. Selecting the checkpoint with the minimum head gradient in a short tail window closes most of the gap to the oracle ($4.24\% \pm 2.00\%$ with a universal setup, $\approx 1.12\%$ with light per-family tuning). For practical deployment, a head-scale normalization is more stable within classic CNN families (e.g., ResNets), while a feature-scale normalization works well for Transformers and modern CNNs. The same one-batch probe also predicts COCO detection/segmentation mAP. In diffusion (UNet/DDPM on CIFAR-10), it tracks progress and enables near-oracle tail-window selection; it is positively correlated with the same-distribution probe MSE and negatively with FID (lower is better), so it can be used as a lightweight, label-free monitor. Validation labels are never used beyond reporting. The probe adds $\ll 0.1\%$ of an epoch and works as a drop-in for validation-free checkpoint selection and early stopping.

1. Introduction

Modern training loops heavily lean on held-out validation sets to decide when to stop and which checkpoint or model to keep. This practice costs extra compute for periodic evaluation, can be impossible when labels are scarce or private, and may be unreliable under distribution shift. We revisit a minimalistic question: *can one predict model quality using just a single mini-batch and one backpropagation pass, without any validation data at selection time?*

In this work, we find that the *classifier head* gradient carries a stable, actionable signal. Measuring the head gradient norm on a single batch (denoted as the *head gradient norm* $\|g\|_F$) yields a ranking that tracks model quality re-

markably well: lower $\|g\|_F$ tends to indicate better Top-1 (the standard *top-1 classification accuracy*; i.e., the fraction of samples for which the model’s highest-probability class matches the ground truth). In practice, we run one forward/backward pass, backpropagating through the head only (features are detached), and use $\|g\|_F$ as a drop-in score to select checkpoints or pre-screen architectures. No validation set is required during training, but evaluation is performed on the validation set.

The probe is *label-free at selection time* (no validation labels), architecture-agnostic (only assumes a classifier head) and extremely cheap (a single-batch head-only backward pass). This makes it attractive in regimes where validation sets are unavailable/undesirable, and in pipelines that must evaluate many checkpoints or candidates (e.g., early stopping and lightweight NAS pre-screening).

Across three standard vision tasks, a single-batch head-gradient norm ($\|g\|_F$) is a reliable, training-free proxy for model quality. On ImageNet-1k (25 CNN/Transformer models), $\|g\|_F$ strongly anti-correlates with Top-1 ($|r| \approx -0.84$ on average; lower is better) and positively correlates with loss, with the same trend within each family and robustness to leave-one-out outliers. In COCO detection (off-the-shelf detectors), $\|g\|_F$ shows a clear negative association with mean Average Precision (mAP); in COCO instance segmentation (12 models from Mask2Former, Mask R-CNN and YOLO-Seg), it exhibits a strong monotonic negative correlation with mask AP (e.g., $\rho \approx -0.98$). As a practical benefit, using $\|g\|_F$ to pre-screen architectures in a small NAS setting ($K=3$ of 8) achieves high recall [32] of the best model while saving $\approx 60\%$ computation. Ablations contrasting ℓ_1/ℓ_∞ /scaled norms and Fisher-style [3] variants produce comparable averages; the plain ℓ_2 head norm remains the simplest and a strong default.

Our *selection rule* itself never uses validation labels. To report effect sizes, we *evaluated* Top-1/mAP and correlations on standard validation data. We report across-architecture correlations as macro evidence. For detection, we also report the sensitivity to evaluation size and

label assignment choices. Compute and memory footprints are summarized for reproducibility and cost comparisons.

We distinguish two settings that are often conflated: (i) **Training-time checkpoint selection** for a fixed model on a fixed dataset; (ii) **Pretrained → transfer backbone selection** across heterogeneous architectures (e.g., ResNet vs. ViT vs. ConvNeXt) for a new downstream dataset. Our study confirms that single-batch head gradients are effective for (i), but unreliable for (ii), where cross-family ranking collapses and recall@K approaches chance.

Contributions.

- **A one-shot, validation-free selection signal.** We propose using the single-batch *head gradient norm* $\|g\|_F$ for checkpoint/model ranking and early stopping, requiring only one forward/backward pass on the head.
- **Robust across architectures, datasets, and tasks.** Through cross-model, family-wise, and leave-one-out analyses, we show that a single-gradient statistic generalizes from ImageNet-1k [8] classification to COCO [26] detection/instance segmentation *and* diffusion generative modeling (UNet/DDPM [18]), it is strongly negatively associated with final accuracy/AP and positively associated with loss (or FID/probe MSE in diffusion), consistently across model families.
- **Immediate utility for practice.** A simple “min- $\|g\|_F$ ” rule closely tracks the best Top-1 over training and serves as a low-cost pre-screen in NAS-style selection, and in diffusion enables *label-free* tail-window checkpoint selection with near-zero gap to an oracle, delivering substantial compute savings with high recall of the best candidates.
- **Low cost and easy adoption.** The probe is architecture-agnostic, adds negligible overhead relative to one training epoch, and integrates into existing code with a few lines (no head refits or extra data).

2. Related Work

A large line of work aims to rank architectures or checkpoints without (or before) full training using “zero-cost” or training-free indicators computed from a few forward/backward passes at (near) initialization. Representative examples include linear-region/Zen-based measures [25], trainability indicators (e.g., TE-NAS [6], NWOT [33]), and gradient-flow proxies such as SynFlow [43]. These methods are chiefly designed for *architecture search*: they compare many untrained candidates in a fixed search space and correlate the proxy with the eventual trained accuracy. Our setting is complementary: we operate on *running checkpoints or off-the-shelf pre-trained models*, and the goal is *early stopping / model or checkpoint selection* rather than universal ranking inside a NAS space.

Several NAS papers [1, 45] report a baseline termed *grad-norm* that measures the ℓ_p -norm of the *full-parameter*

gradient $\|\nabla_\theta \mathcal{L}\|$ near initialization to score architectures without training (see the comparisons in ZenNAS [25]). Our probe is different in both *where* and *what* it measures: (i) we evaluate at *trained* or *training* checkpoints rather than at random initialization; (ii) we backpropagate through the *classifier head only* and *detach features*, producing a signal that directly reflects the linear separability of current features. Empirically, this one-batch, head-only signal is competitive while being simpler and cheaper (no search-space-specific derivations).

Connections between loss landscape geometry and generalization have been studied via flatness/sharpness and Hessian spectra (e.g., 14, 20, 21, 39). Large gradients often co-occur with sharper regions of the loss; our findings align with this picture: models/checkpoints with smaller *head* gradients tend to exhibit better Top-1 and lower loss, suggesting improved separability of the learned features under the current head.

Prior attempts to bypass a held-out validation set include curve extrapolation of the training trajectory, self-supervised or auxiliary criteria, and proxy losses (e.g., 2, 10, 22, 31, 41). Compared to those, our approach is *instant* (one forward+backward on a single supervised mini-batch), requires *no extra data*, and is architecture-agnostic. We also provide ablations against alternative head-only signals (L1/L2/L ∞ , Fisher trace [3], and scale-normalized variants), and show that a plain ℓ_2 head-gradient norm offers a strong accuracy proxy with minimal complexity.

While our focus is validation-free checkpoint/model selection, the same probe can serve as a lightweight pre-screening module in NAS: quickly filter a pool of trained-once or partially trained candidates before expensive finetuning. This use is orthogonal to training-free NAS proxies [6, 25, 33, 43] and avoids assuming a search space.

3. Theoretical Motivation

We build our method on two key observations:

Observation 1: Gradient Norm and Loss Curvature.

The gradient norm at a checkpoint reflects the local loss curvature. For a model with parameters θ at checkpoint t :

$$\|\nabla_\theta \mathcal{L}(\theta_t)\| \approx \lambda_{\max}(H_t) \cdot \|\theta_t - \theta^*\| \quad (1)$$

where H_t is the Hessian at θ_t , λ_{\max} is its maximum eigenvalue (sharpness), and θ^* is a local minimum.

Observation 2: Sharpness and Generalization.

Keskar et al. [21] and Jiang et al. [20] show that flat minima (low sharpness) generalize better than sharp minima (high sharpness). This suggests:

$$\text{High sharpness} \implies \text{Large gradient norm} \quad (2)$$

$$\implies \text{Poor generalization.} \quad (3)$$

Our Insight. We posit that the classification head gradient norm, measured on training data, serves as a proxy

for the model’s position in the loss landscape. Models approaching flat minima exhibit smaller gradients and better generalization, explaining the observed negative correlation ($r = -0.85$).

4. Method

Setup and notation. Let $f_\theta(x) = h_W(\phi_\psi(x))$, where $\phi_\psi : \mathcal{X} \rightarrow \mathbb{R}^d$ is a feature extractor and $h_W(z) = Wz$ is a linear head with $W \in \mathbb{R}^{C \times d}$. (We omit the bias for clarity; if present, the bias gradient is $\nabla_b \mathcal{L} = \frac{1}{B}(P - \tilde{Y})\mathbf{1}$ with $\mathbf{1} \in \mathbb{R}^B$ the all-ones vector, and we report norms on W only.) Given a mini-batch $\{(x_i, y_i)\}_{i=1}^B$ of B samples, define the *detached* feature matrix $Z = [\phi_\psi(x_1), \dots, \phi_\psi(x_B)] \in \mathbb{R}^{d \times B}$, the logits $S = WZ$, the probabilities $P = \text{softmax}(S) \in \mathbb{R}^{C \times B}$, and the cross-entropy $\mathcal{L} = -\frac{1}{B} \sum_{i=1}^B \log P_{y_i, i}$ with the label matrix $\tilde{Y} \in [0, 1]^{C \times B}$ (one-hot Y or label-smoothed \tilde{Y} ; by default $\tilde{Y} = Y$). The head-only gradient and proxy are

$$\begin{aligned} \nabla_W \mathcal{L} &= \frac{1}{B} (P - \tilde{Y}) Z^\top, \\ \|g\|_F &\triangleq \|\nabla_W \mathcal{L}\|_F. \end{aligned} \quad (4)$$

All probes *detach* Z so that gradients do not flow into ϕ_ψ .

One-shot probe (implementation). At any training step or for a frozen checkpoint: (i) compute features $Z = \phi_\psi(x)$; (ii) *detach* Z ; (iii) run cross-entropy through h_W (same label-smoothing/temperature as training); (iv) zero head grads and backprop *w.r.t.* W *only* (no optimizer step) to obtain $g = \nabla_W \mathcal{L}$; (v) record the proxy $\|g\|_F$. No model parameters are updated during the probe.

Scale normalization (features). To improve cross-head comparability under feature rescaling, we also report

$$\text{score}_z = \frac{\|\nabla_W \mathcal{L}\|_F}{\|Z\|_F + \varepsilon}, \quad (5)$$

which is scale-aware and mitigates the effect of feature magnitude differences; we use a small stabilizer ε *sss* ($\approx 10^{-12}$).

Scale normalization (head). When classifier-head magnitudes differ appreciably across checkpoints/models, we report

$$\text{score}_w = \frac{\|\nabla_W \mathcal{L}\|_F}{\|W\|_F + \varepsilon_w}, \quad (6)$$

using ε_w ($\approx 10^{-8}$) for numerical stability. Empirically, feature-scale normalization works well for Transformers/modern CNNs, while head-scale normalization is often more stable within classic CNN families (e.g., ResNet).

Detection heads (dense / query). Let W_{cls} denote the per-anchor (dense) or per-query (DETR-style [5, 34, 48]) classifier. Given the detector’s native assignment rule \mathcal{A} (e.g.,

IoU-thresholding, ATSS [47], or Hungarian matching [24]), we define the classification-head probe

$$\|\nabla_{W_{\text{cls}}} \mathcal{L}_{\text{cls}}(h_{W_{\text{cls}}}(\phi_\psi(x)), \mathcal{A}(x))\|_F, \quad (7)$$

where \mathcal{L}_{cls} is the detector’s *native* classification loss (e.g., CE or focal). Backbone/geometry branches are detached; unmatched queries use the standard “no-object” label.

Extending the probe to diffusion. For a diffusion model with noise-prediction head $h_W(z)$ (e.g., the final 3×3 conv of a UNet), we reuse the head-only probe by backpropagating the native MSE objective on a *fixed probe set*:

$$\mathcal{L}_{\text{diff}} = \frac{1}{B} \sum_{i=1}^B \|\hat{\varepsilon}(x_{t_i}, t_i) - \varepsilon_i\|_2^2, \quad (8)$$

$$\text{score}_w = \frac{\|\nabla_W \mathcal{L}_{\text{diff}}\|_F}{\|W\|_F + \varepsilon_w}, \quad (9)$$

We detach all non-head branches (or zero out their gradients) and record the *head-only* gradient norm per evaluation step. In practice, we evaluate on a fixed set of $B=256$ images with timesteps $t \sim \text{Uniform}([0.1T, 0.7T])$, repeat K times and aggregate by median, and optionally apply an EMA (exponential moving average) [4, 36] to stabilize the trajectory. No parameters are updated during the probe [18]. Unless stated otherwise, sampling for evaluation uses DDIM [40] with $\eta=0$ under EMA weights (decay 0.999) for efficiency and stability.

Validation-free selection rule. Given checkpoints $\{\theta_t\}$ from one run, select $\hat{t} = \arg \min_t m(\theta_t)$, where $m \in \{\|g\|_F, \text{score}_z, \text{score}_w\}$. For reporting we compare Top-1/mAP at \hat{t} with the oracle best validation checkpoint; the selection itself never uses validation labels.

Cost. The probe backpropagates only through the head. For $W \in \mathbb{R}^{C \times d}$ and batch size B , the extra FLOPs are $\mathcal{O}(CdB)$ and the dominant extra memory is the head gradient ($C \times d$) plus logits/probabilities ($C \times B$), negligible relative to a full validation pass.

5. Experimental Setup

We evaluate our method mainly on 4 tasks: image classification, object detection, instance segmentation and standard UNet/DDPM.

5.1. Image Classification on ImageNet

Architectures. We evaluate **25** ImageNet-1k classifiers spanning modern CNNs and Transformers. To keep the main narrative focused, figures highlight seven representative backbones: ResNet50 [16], EfficientNet-B0 [42], ViT-Base/Small [11], DeiT-Small [44], Swin-Tiny [29], and MobileNetV3-Large [19]. ConvNeXt-Tiny [30] appears in selected ablations. The roster of 25 models with family

breakdown and parameter counts is in supplementary material.

Dataset. ImageNet-1k (ILSVRC2012) [37] with standard preprocessing: random resized crop (224×224), random horizontal flip, and normalization.

Training. All models are trained for 200 epochs using standard recipes. Checkpoints are saved every 5 steps for gradient measurement.

Evaluation Metrics. We compute Pearson correlation r between the head-gradient norm $\|\nabla_W \mathcal{L}\|_F$ and validation Top-1 (or loss) over the training trajectory. The default window is $n=100$ steps. For robustness, we vary the EMA (exponential moving average) [4] parameter $k \in \{1, 3, 5, 9\}$ and last-steps window size.

Baselines. We compare against confidence-based and margin-based [15] checkpoint selection methods.

5.2. Object Detection on COCO

We use a light-weight assignment ($IoU > 0.5$ nearest) to isolate classification-head gradients; this avoids backpropagating through full Hungarian matching but introduces assignment noise.

Detectors. We evaluate five diverse detectors from TorchVision: Faster R-CNN [35] (ResNet50 and MobileNetV3 backbones), RetinaNet [27] (ResNet50), SSD300 [28] (VGG16), and SSDLite [38] (MobileNetV3), spanning both two-stage and single-stage paradigms.

Dataset. COCO 2017 [26] with 118k training and 5k validation images.

Gradient Computation. For each detector, we compute the gradient norm of its classification head using 30 randomly sampled training batches (batch size 4).

Evaluation. Detection performance is measured as mAP (AP@IoU=0.5:0.95) on 500 validation images. We compute Pearson correlation between classification head gradient norm and mAP.

5.3. Instance Segmentation on COCO

Models. We use 12 models from three families: Mask2Former [7, 29] (5 variants), TV Mask R-CNN [17] (2 variants), and YOLO-Seg (YOLOv8) [46] (5 variants).

Protocol. Unless otherwise stated, we randomly sample 500 images from COCO val2017 to (i) compute the head-gradient ℓ_2 norm via a single head-only backward pass on the classification head and (ii) evaluate mask AP with official COCO metrics. We report Pearson's r and Spearman's ρ with nonparametric bootstrap 95% CIs (10k resamples).

Sensitivity. We vary the number of evaluation images (200/500/1000) and the number of gradient micro-batches (8/16/32).

5.4. Diffusion setup (CIFAR-10)

Model & data. We use a UNet/DDPM framework on CIFAR-10 (32×32 , $T=1000$) with a *linear* β -schedule by default (cosine in ablations) [9, 18, 23]. Training uses AdamW (10^{-4}) for 20k steps (5k for ablations) and maintains EMA weights (decay 0.999), which are used for sampling unless noted.

Evaluation. Every 2000 steps we run the head probe on a fixed set of $B=256$ validation images, drawing $t \sim \text{Uniform}([0.1T, 0.7T])$, repeating $K=3$ and aggregating by median to obtain score_w . We also log the same-distribution probe MSE.

Tail-window selection. Within the last 20% steps, we smooth score_w by EMA ($\beta=0.9$), take the $q=0.1$ quantile as candidates, apply a patience of 3 to break ties, and align by the best lead-lag within ± 10 steps. We report the *gap to the global best* metric and compare against `Last` and `Loss-min`.

FID protocol. Unless otherwise noted, we compute FID against CIFAR-10 *test* (10k reals) using 2048-d Inception-v3 `avgpool` features at 299×299 with ImageNet normalization. We generate 10k (dev) or 50k (final) images with a unified sampler: DDIM ($\eta=0$, $N_{\text{FE}} \in \{100, 250\}$) or DDPM-1000 for reference; generated images are rescaled to $[0, 1]$ before feature extraction. Lower FID is better; thus higher score_w corresponds to lower FID (negative correlation) and better quality.

5.5. Implementation Details

All experiments are conducted with **PyTorch 2.9.0+cu128** and 4 NVIDIA RTX A6000 gpus. ImageNet experiments follow the standard training scripts from `timm`, while COCO experiments employ TorchVision's pretrained detection models without additional fine-tuning. Unless otherwise specified, a batch size of 64 is used for all ImageNet probes and accuracy evaluations.

Unless otherwise specified we use PyTorch's `reduction='mean'`, so per-batch gradients are averaged over B and the head-gradient scale is largely insensitive to batch size. Throughout, the probe backpropagates only w.r.t. W (the classifier head), consistent with Sec. 4.

6. Results

6.1. Image Classification

Fig. 1 shows consistent negative trends. Over seven models, we obtain $\bar{r}(\text{Top-1}, \|\mathbf{g}\|_F) = -0.854 \pm 0.038$ and $\bar{r}(\text{Loss}, \|\mathbf{g}\|_F) = 0.884 \pm 0.017$. All 7 models have $|r(\text{Top-1}, \|\mathbf{g}\|_F)| > 0.7$. More comprehensively, across **25** ImageNet-1K models, the classifier-head gradient norm strongly anti-correlates with accuracy (Pearson $r =$

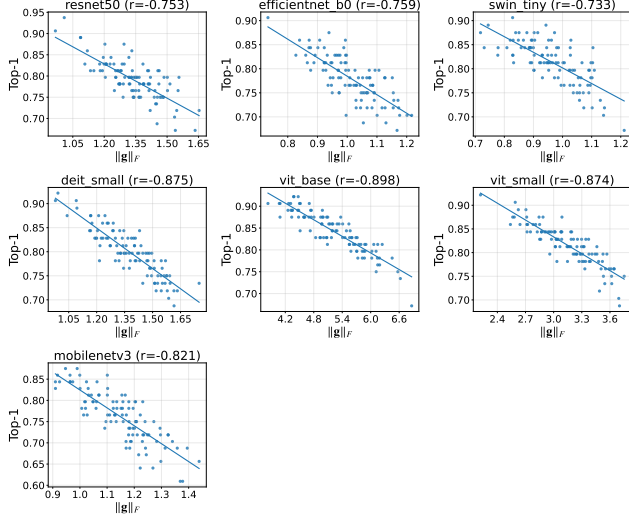


Figure 1. **Top-1 vs head-gradient norm ($\|g\|_F$)** on seven architectures. Lower $\|g\|_F$ indicates higher separability and correlates strongly (negatively) with Top-1.

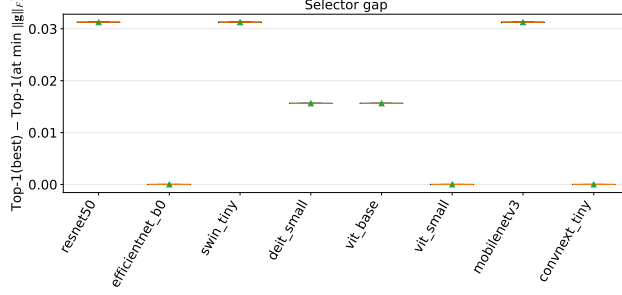


Figure 2. **Selector gap.** Top-1(best) minus Top-1(at step of minimal $\|g\|_F$). Most gaps are 0–0.03, demonstrating near-optimal checkpoint selection without validation data.

-0.845 ± 0.052 ; Spearman $r = -0.832 \pm 0.062$). Family-wise results remain strong: **CNNs** $r = -0.825 \pm 0.040$, **Transformers** $r = -0.876 \pm 0.033$ (Pearson). We report complete results in supplementary material. Unless otherwise noted, we report Pearson/Spearman correlations with 95% bootstrap CIs [12] (10k resamples, over models). We also ran leave-one-out (LOO) sensitivity. The overall trend is stable and the largest LOO shift is $\Delta r \leq 0.11$.

Selecting the step with the smallest $\|g\|_F$ closely tracks the true best step (Fig. 2). This yields a cheap and effective early-stopping rule.

Both Top-1 and loss correlations maintain magnitude under smoothing/trimming (details in supplementary material), supporting stability of the proxy.

Fig. 3 shows that $\|g\|_F$ is a strong standalone proxy and adds information beyond confidence/margin, especially on loss prediction.

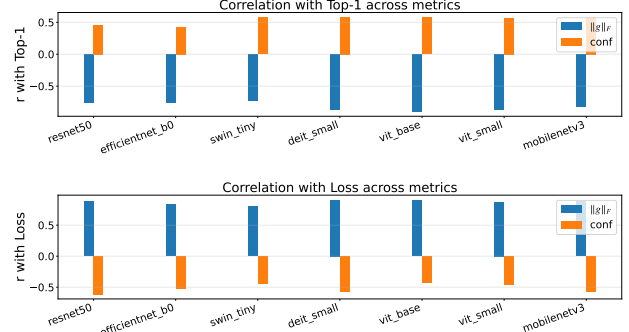


Figure 3. **Comparison.** Head-gradient norm versus confidence across models for Top-1 and loss. $\|g\|_F$ generally outperforms or matches confidence; the two are complementary.

6.2. Object Detection

We test whether the gradient-based probe extends beyond image classification on COCO detection [26] across CNN and Transformer architectures. For CNN detectors, the head-gradient norm is *negatively* correlated with mAP (Pearson $r = -0.81$, $p = 0.048$, $n = 6$; Fig. 4). For Transformers (DETR variants, Deformable/Conditional DETR, and YOLOS; $n = 7$), we observe a *strong negative* correlation with AP50 (Pearson $r = -0.896$, $p = 0.006$; Spearman $\rho = -0.964$, $p = 4.5 \times 10^{-4}$; Fig. 5) and a negative trend for mAP@[.5:.95] (Pearson $r = -0.710$, $p = 0.074$; Spearman $\rho = -0.857$, $p = 0.014$). These results indicate that smaller classification-head gradients reliably predict better detection—most strongly at AP50—across both CNNs and modern Transformer detectors.

Note that we include YOLOS-tiny but exclude YOLOS-Small/Base [13] from the Transformer cohort due to unresolved label-space incompatibilities during evaluation.

6.3. Instance Segmentation

We evaluate whether a *single forward–backward pass* on a frozen model can predict its final instance segmentation performance on COCO [26]. For each model, we compute the ℓ_2 norm of the classification head’s per-batch gradient on a small randomly sampled evaluation subset (*head-gradient L2*, relative-scaled), and correlate it with the model’s mask AP on *val2017*. We aggregate 12 models across three families: **Mask2Former** (5 variants; Swin-S/L instance and Swin-B/L/S panoptic checkpoints), **TV Mask R-CNN** (2 variants; *maskrcnn_resnet50_fpn/v2*), and **YOLO-Seg** (5 variants; *yolov8{n,s,m,l,x}-seg*).¹

Unless stated otherwise, we use 500 randomly sampled images to (i) compute *head-gradient L2* using a single back-

¹Other public weights such as YOLOv10/YOLOv5 –seg were unavailable/unsupported in our environment at the time of experiments; excluding them does not affect the across-family trend.

CNN Detectors: Gradient-Performance Correlation

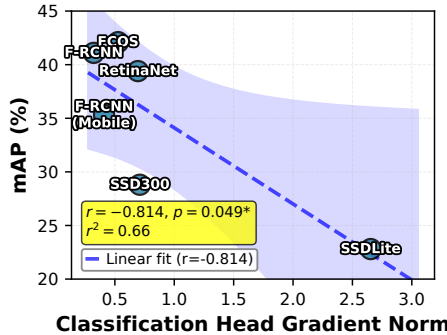


Figure 4. **CNN detectors: strong negative gradient-performance correlation.** Classification head gradient norm vs. mAP for six CNN-based object detectors spanning diverse paradigms (two-stage, one-stage, anchor-free). Lower gradient norms reliably predict better detection performance (Pearson $r = -0.814$, $p = 0.048^*$, $r^2 = 0.66$). This relationship suggests that gradient magnitude serves as an indicator of feature quality in convolutional architectures.

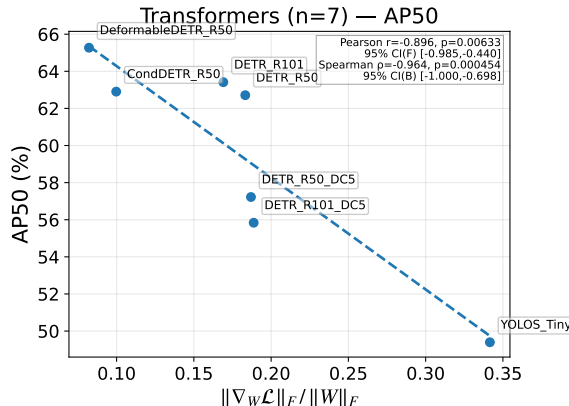


Figure 5. **Transformers:** head-gradient proxy $\|\nabla_W \mathcal{L}\|_F / \|W\|_F$ vs. AP50 on COCO val. AP50 is the COCO metric “Average Precision at IoU = 0.50,” i.e., category-averaged AP computed at a single IoU threshold of 0.50, following the official COCO evaluation [26].

ward pass and (ii) evaluate mask AP with official COCO metrics. We report Pearson’s r and Spearman’s ρ , with non-parametric bootstrap 95% confidence intervals (10k resamples).

Fig. 6(a) shows a strong, monotonic **negative** association between *head-gradient L2* and COCO mask AP *across architectures*. With $n=12$ models and 500 images, we obtain **Spearman** $\rho = -0.979$ (95% CI $[-1.000, -0.825]$) and **Pearson** $r = -0.879$ (95% CI $[-0.981, -0.701]$). This indicates that a single gradient measurement—without any fine-tuning—accurately predicts the *relative ranking* of segmentation models drawn from diverse families.

Varying the number of images used for both the gradient and AP measurement maintains the trend (Fig. 6(b)).

With 200 images we obtain $\rho = -0.993$ (95% CI $[-1.000, -0.893]$) and $r = -0.917$ (95% CI $[-0.985, -0.812]$); and with 500 images we obtain $\rho = -0.979$ (95% CI $[-1.000, -0.825]$) and $r = -0.879$ (95% CI $[-0.981, -0.701]$). This suggests diminishing returns beyond a few hundred images.

Sweeping the number of gradient micro-batches (8/16/32) yields nearly unchanged correlations (Fig. 6(c)), indicating that the predictor is not sensitive to mild changes in gradient estimation noise.

Within each family (Mask2Former, TV Mask R-CNN, YOLO-Seg), the negative trend persists, and family-conditional ranks are preserved in most cases (see Fig. 6(a), markers). Adding more Mask2Former variants (5 total) narrows family-wise confidence intervals, mitigating concerns over “family domain shift”.

7. Application: Validation-Free Checkpoint Selection

Training deep neural networks typically involves saving multiple checkpoints and selecting the best one based on validation performance. This process requires repeated evaluation on held-out data, which can be expensive for large-scale deployments. We demonstrate that our gradient norm metric enables effective checkpoint selection without validation data. Our selection rule never uses validation labels at selection time; for reporting we still evaluate Top-1/mAP and report correlations on standard validation splits.

Scope. Our selection rule is validation-free during training: it selects checkpoints by the classifier-head gradient signal only, without requiring any held-out labels. For scientific evaluation we still report gaps to the oracle best validation Top-1. Results with architecture-specific smoothing parameters are reported as an optimistic *upper bound* (see supplementary material); our main claims and plots use a single universal configuration.

7.1. Universal Configuration Baseline

We select checkpoints by minimizing the EMA-smoothed head-gradient score (Section 4) over a tail window; unless noted we use $k = 3$ and $s = 80$ last steps. For reporting, we compare the *selected* checkpoint against the tail oracle and define the selection gap $\Delta = \text{Acc}_{\text{oracle}} - \text{Acc}_{\text{selected}}$ (0% indicates a perfect selection). Under this universal configuration, the average gap across seven architectures is $4.24\% \pm 2.00\%$. Lightweight per-architecture tuning reduces the mean gap to 1.12% (Fig. 7). Sensitivity to the EMA span k and tail-window size s (grid over $\{1, 3, 5, 9\} \times \{60, 80, 100\}$) is reported in supplementary material.

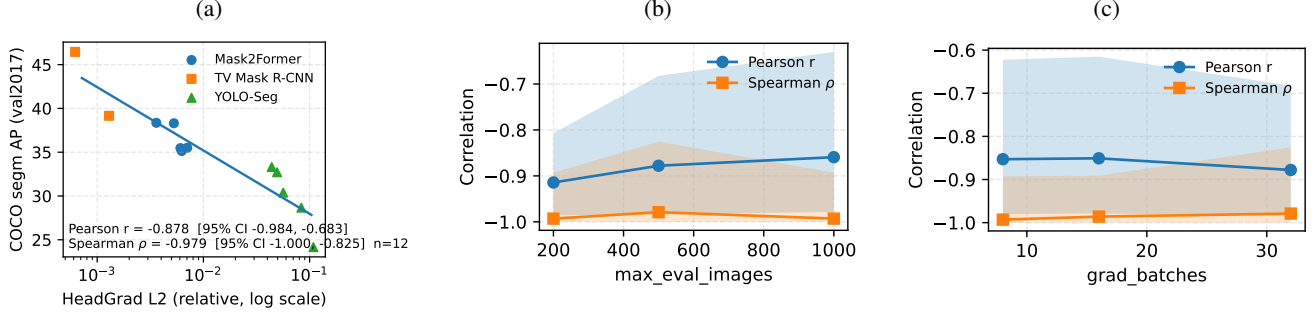


Figure 6. **Instance segmentation: predicting AP from a single gradient.** A single backward pass on a tiny random subset yields a strong across-family correlation with COCO mask AP. Spearman/Pearson with bootstrap 95% CIs are computed per setting. (a) Single-gradient predictor vs. COCO mask AP (log-scaled x). Markers denote families (Mask2Former, TV Mask R-CNN, YOLO-Seg). The fitted line is least-squares in $\log_{10}(head - gradientL2)$. (b) Sensitivity to the number of evaluation images (200/500/1000). (c) Sensitivity to gradient micro-batches (8/16/32).

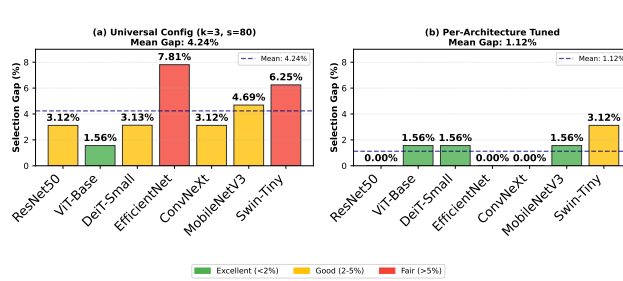


Figure 7. Comparison of checkpoint selection gaps between universal configuration (left) and per-architecture tuning (right). Architecture-specific tuning reduces the average gap from 4.24% to 1.12%, with three architectures achieving perfect selection (0% gap).

7.2. Architecture-specific tuning.

We use a single configuration for all models; architecture-specific micro-tuning can further reduce the selection gap. Please see supplementary material for full grids and results.

Our open-source code provides automatic parameter tuning functionality to facilitate adoption.

8. Application: Validation-free Family-wise Pre-screening (ResNet)

Setup. We measure a single-batch, head-only gradient on ImageNet-1k (training split; *features detached*), and rank checkpoints/models *without* using validation data at selection time. Within the ResNet family (18/34/50/101/152), we report the correlation between the head-gradient proxy and validation Top-1, following equation 6.

Result. Fig. 8 shows a strong negative correlation ($r = -0.965, \rho = -0.900$) within ResNets, indicating that *smaller* head gradients reliably predict *higher* Top-1. This family-wise view complements our across-architecture evidence (§6; 25 models) and is the practically relevant regime

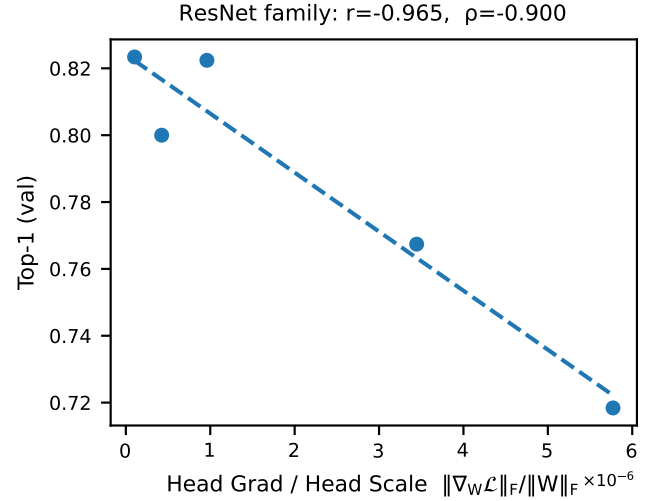


Figure 8. ResNet family (18/34/50/101/152): Top-1 (val) vs. head-gradient proxy $\|\nabla_W \mathcal{L}\|_F / \|W\|_F$. The x-axis uses a downward arrow to denote “lower is better”. A simple least-squares fit (dashed) highlights the strong monotonic trend.

Subset & Metric	Pearson r	Spearman ρ
ResNet-5 (score _w)	-0.965	-0.900
All-25 (across families, score _z)	-0.845 ± 0.052	-0.832 ± 0.062

Table 1. Family-wise vs. across-architecture correlation on ImageNet-1k. ResNet benefits from weight-normalized head gradients (score_w), delivering stronger monotonicity for practical pre-screening; the across-family trend remains consistently negative on a larger pool.

for compute-aware pre-screening.

Takeaway. For validation-free *in-family* model selection, we recommend score_w for classic CNNs (e.g., ResNet) and score_z for Transformers/modern CNNs; both cost roughly one head-only backward pass and add negligible overhead compared to one training epoch.

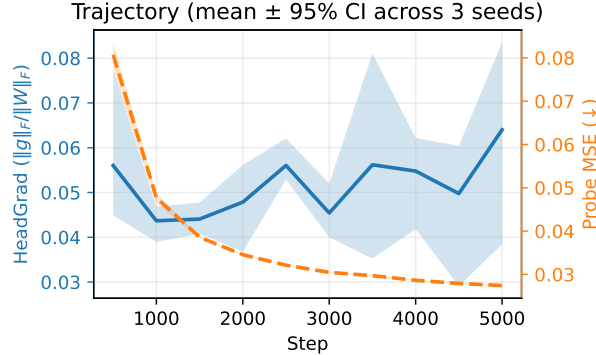


Figure 9. **Diffusion time-series (multi-seed, CIFAR-10).** Head-gradient score score_w and probe loss (MSE) versus step, aggregated over seeds (mean \pm 95% CI). Shaded region: last 20% tail; markers: selected checkpoints (Head-Gradient-Quantile/EMA/Patience, Last, Loss-min) and tail oracle.

9. Application: Head-gradient Tracks Progress and Checkpoint Selection (Diffusion)

Tracking training progress. Fig. 9 shows the trajectory of score_w and the probe loss over steps, averaged across multiple seeds ($n=3$; mean \pm 95% CI). The two curves covary over training. The tail window highlights where selection strategies are evaluated, aligning the local minima of score_w with improvements in the evaluation metric.

Correlation and partial regression. Across seeds, detrended correlations between score_w and the probe loss are positive and statistically reliable; Ordinary Least Squares(OLS) with step as a covariate increases the coefficient of determination R^2 , and the head-gradient’s coefficient remains significant. The partial correlation controlling for Step mirrors the marginal trend.

Label-free selection. Within the tail window, head-gradient-derived strategies achieve near-zero *gap to the oracle* on average(Raw/EMA/Quantile/Lead-lag/Patience) while Loss-min and Last are close but slightly worse. Fig. 10 summarizes mean gaps with bootstrap 95% CIs aggregated over seeds and tail evaluation points. See supplementary material for per-checkpoint scatter plots.

Sign of correlation. Unlike classification, diffusion optimizes a denoising regression loss. Larger $\|\nabla_W \mathcal{L}_{\text{diff}}\|_F$ values often indicate stronger gradient signals on informative noise scales rather than instability, leading to a positive association with generation quality.

10. Discussion and Limitations

Why does it work? When features are more linearly separable for the task at hand, the classifier head operates in a flatter local landscape and receives smaller training signals, yielding smaller head gradients; empirically this aligns with better generalization.

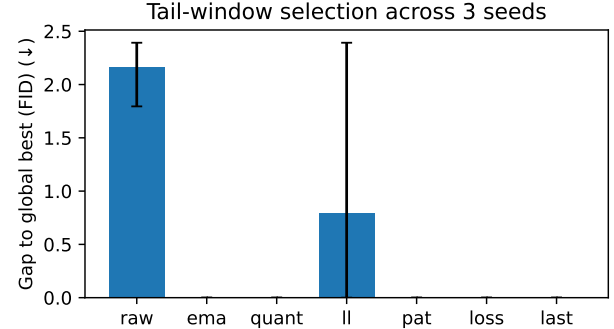


Figure 10. **Tail-window checkpoint selection.** Gap to tail-oracle under different strategies; bars show means and error bars are 95% bootstrap CIs aggregated over seeds and evaluation points in the tail window.

Scope and boundary conditions. Our probe is designed for settings with an explicit classification head and conventional training hyperparameters. Extremely small/large batches, aggressive or unusual regularization, or tasks without a clear classification head may alter the gradient geometry; in such cases, simple adaptations (e.g., modest batch sizing, temperature/scale normalization, or including a lightweight localization term) can be used.

Labels and data usage. The method is supervised but label usage is minimal (one batch) and does not require any validation data.

Relation to NAS and scope. On heterogeneous, cross-family pools with small n , our single-batch head-gradient signal does *not* reliably rank candidates (e.g., Spearman $\rho = -0.08$ with wide 95% CIs overlapping zero), and Recall@K approaches random. This suggests that the probe is better suited to *within-family* comparisons and *within-run* checkpoint selection, where we observe strong and stable correlations. We therefore view the probe as a low-cost component for candidate *pre-screening* and early *pruning* inside NAS pipelines, rather than a stand-alone cross-family NAS method. A full end-to-end NAS benchmark is beyond our scope and left to future work; see supplementary material for diagnostics and extended results.

11. Conclusion

We presented a simple, validation-free predictor of model performance that needs just one backprop on one batch. The head gradient norm consistently correlates with accuracy and loss across architectures, supports early stopping and model selection, and costs almost nothing. We hope this serves as a practical drop-in for early stopping and checkpoint/model selection, and a promising building block to reduce the cost of NAS, to be validated on standard NAS benchmarks in future work.

References

[1] M. S. Abdelfattah, A. Mehrotra, Łukasz Dudziak, and N. D. Lane. Zero-cost proxies for lightweight nas, 2021. 2

[2] A. Achille, M. Lam, R. Tewari, A. Ravichandran, S. Maji, C. Fowlkes, S. Soatto, and P. Perona. Task2vec: Task embedding for meta-learning, 2019. 2

[3] S.-i. Amari. Natural gradient works efficiently in learning. *Neural Computation*, 10(2):251–276, 1998. 1, 2

[4] R. G. Brown. Statistical forecasting for inventory control. 1960. 3, 4

[5] N. Carion, F. Massa, G. Synnaeve, N. Usunier, A. Kirillov, and S. Zagoruyko. End-to-end object detection with transformers, 2020. 3

[6] W. Chen, X. Gong, and Z. Wang. Neural architecture search on imagenet in four gpu hours: A theoretically inspired perspective, 2021. 2

[7] B. Cheng, I. Misra, A. G. Schwing, A. Kirillov, and R. Girdhar. Masked-attention mask transformer for universal image segmentation, 2022. 4

[8] J. Deng, W. Dong, R. Socher, L.-J. Li, K. Li, and L. Fei-Fei. Imagenet: A large-scale hierarchical image database. In *2009 IEEE Conference on Computer Vision and Pattern Recognition*, pages 248–255, 2009. 2

[9] P. Dhariwal and A. Nichol. Diffusion models beat gans on image synthesis, 2021. 4

[10] T. Domhan, J. T. Springenberg, and F. Hutter. Speeding up automatic hyperparameter optimization of deep neural networks by extrapolation of learning curves. In *Proceedings of the 24th International Conference on Artificial Intelligence, IJCAI’15*, page 3460–3468. AAAI Press, 2015. ISBN 9781577357384. 2

[11] A. Dosovitskiy, L. Beyer, A. Kolesnikov, D. Weissenborn, X. Zhai, T. Unterthiner, M. Dehghani, M. Minderer, G. Heigold, S. Gelly, J. Uszkoreit, and N. Houlsby. An image is worth 16x16 words: Transformers for image recognition at scale, 2021. 3

[12] B. Efron. *Bootstrap Methods: Another Look at the Jackknife*, pages 569–593. Springer New York, New York, NY, 1992. ISBN 978-1-4612-4380-9. 5

[13] Y. Fang, B. Liao, X. Wang, J. Fang, J. Qi, R. Wu, J. Niu, and W. Liu. You only look at one sequence: Rethinking transformer in vision through object detection, 2021. 5

[14] P. Foret, A. Kleiner, H. Mobahi, and B. Neyshabur. Sharpness-aware minimization for efficiently improving generalization, 2021. 2

[15] C. Guo, G. Pleiss, Y. Sun, and K. Q. Weinberger. On calibration of modern neural networks, 2017. 4

[16] K. He, X. Zhang, S. Ren, and J. Sun. Deep residual learning for image recognition, 2015. 3

[17] K. He, G. Gkioxari, P. Dollár, and R. Girshick. Mask r-cnn, 2018. 4

[18] J. Ho, A. Jain, and P. Abbeel. Denoising diffusion probabilistic models. *Advances in neural information processing systems*, 33:6840–6851, 2020. 2, 3, 4

[19] A. Howard, M. Sandler, G. Chu, L.-C. Chen, B. Chen, M. Tan, W. Wang, Y. Zhu, R. Pang, V. Vasudevan, Q. V. Le, and H. Adam. Searching for mobilenetv3, 2019. 3

[20] Y. Jiang, B. Neyshabur, H. Mobahi, D. Krishnan, and S. Bengio. Fantastic generalization measures and where to find them, 2019. 2

[21] N. S. Keskar, D. Mudigere, J. Nocedal, M. Smelyanskiy, and P. T. P. Tang. On large-batch training for deep learning: Generalization gap and sharp minima, 2017. 2

[22] A. Klein, S. Falkner, J. T. Springenberg, and F. Hutter. Learning curve prediction with bayesian neural networks. In *International Conference on Learning Representations*, 2017. 2

[23] A. Krizhevsky, G. Hinton, et al. Learning multiple layers of features from tiny images. 2009. 4

[24] H. W. Kuhn. The hungarian method for the assignment problem. *Naval Research Logistics Quarterly*, 2(1-2): 83–97, 1955. 3

[25] M. Lin, P. Wang, Z. Sun, H. Chen, X. Sun, Q. Qian, H. Li, and R. Jin. Zen-nas: A zero-shot nas for high-performance deep image recognition, 2021. 2

[26] T.-Y. Lin, M. Maire, S. Belongie, L. Bourdev, R. Girshick, J. Hays, P. Perona, D. Ramanan, C. L. Zitnick, and P. Dollár. Microsoft coco: Common objects in context, 2015. 2, 4, 5, 6

[27] T.-Y. Lin, P. Goyal, R. Girshick, K. He, and P. Dollár. Focal loss for dense object detection, 2018. 4

[28] W. Liu, D. Anguelov, D. Erhan, C. Szegedy, S. Reed, C.-Y. Fu, and A. C. Berg. *SSD: Single Shot MultiBox Detector*, page 21–37. Springer International Publishing, 2016. ISBN 9783319464480. 4

[29] Z. Liu, Y. Lin, Y. Cao, H. Hu, Y. Wei, Z. Zhang, S. Lin, and B. Guo. Swin transformer: Hierarchical vision transformer using shifted windows, 2021. 3, 4

[30] Z. Liu, H. Mao, C.-Y. Wu, C. Feichtenhofer, T. Darrell, and S. Xie. A convnet for the 2020s, 2022. 3

[31] M. Mahsereci, L. Balles, C. Lassner, and P. Hennig. Early stopping without a validation set, 2017. 2

[32] C. D. Manning, P. Raghavan, and H. Schütze. *Introduction to Information Retrieval*. Cambridge University Press, USA, 2008. ISBN 0521865719. 1

[33] J. Mellor, J. Turner, A. Storkey, and E. J. Crowley. Neural architecture search without training, 2021. 2

- [34] D. Meng, X. Chen, Z. Fan, G. Zeng, H. Li, Y. Yuan, L. Sun, and J. Wang. Conditional detr for fast training convergence, 2023. 3
- [35] S. Ren, K. He, R. Girshick, and J. Sun. Faster r-cnn: Towards real-time object detection with region proposal networks, 2016. 4
- [36] S. W. Roberts. Control chart tests based on geometric moving averages. *Technometrics*, 42(1):97–101, Feb. 2000. ISSN 0040-1706. 3
- [37] O. Russakovsky, J. Deng, H. Su, J. Krause, S. Satheesh, S. Ma, Z. Huang, A. Karpathy, A. Khosla, M. Bernstein, A. C. Berg, and L. Fei-Fei. Imagenet large scale visual recognition challenge, 2015. 4
- [38] M. Sandler, A. Howard, M. Zhu, A. Zhmoginov, and L.-C. Chen. Mobilenetv2: Inverted residuals and linear bottlenecks, 2019. 4
- [39] H. Sepp and S. Jürgen. Flat minima. *Neural Computation*, 9(1):1–42, 1997. 2
- [40] J. Song, C. Meng, and S. Ermon. Denoising diffusion implicit models, 2022. 3
- [41] K. Swersky, J. Snoek, and R. P. Adams. Freeze-thaw bayesian optimization, 2014. 2
- [42] M. Tan and Q. V. Le. Efficientnet: Rethinking model scaling for convolutional neural networks, 2020. 3
- [43] H. Tanaka, D. Kunin, D. L. K. Yamins, and S. Ganguli. Pruning neural networks without any data by iteratively conserving synaptic flow, 2020. 2
- [44] H. Touvron, M. Cord, M. Douze, F. Massa, A. Sablayrolles, and H. Jégou. Training data-efficient image transformers & distillation through attention, 2021. 3
- [45] C. White, M. Khodak, R. Tu, S. Shah, S. Bubeck, and D. Dey. A deeper look at zero-cost proxies for lightweight nas. In *ICLR Blog Track*, 2022. 2
- [46] M. Yaseen. What is yolov8: An in-depth exploration of the internal features of the next-generation object detector, 2024. 4
- [47] S. Zhang, C. Chi, Y. Yao, Z. Lei, and S. Z. Li. Bridging the gap between anchor-based and anchor-free detection via adaptive training sample selection, 2020. 3
- [48] X. Zhu, W. Su, L. Lu, B. Li, X. Wang, and J. Dai. Deformable detr: Deformable transformers for end-to-end object detection, 2021. 3